
Electrocardiogram Instruction Tuning for Report Generation

Zhongwei Wan^{1†*} Che Liu^{3†} Xin Wang¹ Chaofan Tao⁵ Hui Shen¹ Zhenwu Peng⁴ Jie Fu⁶
Rossella Arcucci³ Huaxiu Yao^{2‡} Mi Zhang^{1*‡}

¹The Ohio State University ²University of North Carolina at Chapel Hill ³Imperial College London

⁴King's College London ⁵HKU ⁶HKUST

*Correspondence to: Zhongwei Wan<wan.512@osu.edu> Mi Zhang<mizhang.1@osu.edu>

†Core contribution ‡Core advising

Abstract

Electrocardiogram (ECG) serves as the primary non-invasive diagnostic tool for cardiac conditions monitoring, are crucial in assisting clinicians. Recent studies have concentrated on classifying cardiac conditions using ECG data but have overlooked ECG report generation, which is not only time-consuming but also requires clinical expertise. To automate ECG report generation and ensure its versatility, we propose the **Multimodal ECG Instruction Tuning (MEIT)** framework, the *first* attempt to tackle ECG report generation with LLMs and multimodal instructions. To facilitate future research, we establish a benchmark to evaluate MEIT with various LLMs backbones across two large-scale ECG datasets. Our approach uniquely aligns the representations of the ECG signal and the report, and we conduct extensive experiments to benchmark MEIT with nine open source LLMs, using more than 800,000 ECG reports. MEIT's results underscore the superior performance of instruction-tuned LLMs, showcasing their proficiency in *quality report generation*, *zero-shot capabilities*, and *resilience to signal perturbation*. These findings emphasize the efficacy of our **MEIT**¹ framework and its potential for real-world clinical application.

1. Introduction

Diagnosing heart diseases is of paramount importance, requiring the analysis of multimodal data sources, which includes electrocardiogram (ECG) recordings and clinical reports. Cardiologists read and interpret these ECG recordings to manually generate comprehensive ECG reports for heart disease diagnosis, which is a complex and time-consuming process. Recently, artificial intelligence (AI) models have

been developed to facilitate ECG data analysis by categorizing ECG data (Chen et al., 2022a; Hu et al., 2023; Liu et al., 2023a; Li et al., 2023b). Despite these early efforts, the automatic generation of reports from ECG recordings remains an underexplored area. Unlike other AI-empowered medical report generation applications (e.g., radiology report), the primary challenges for ECG report generation stem from the distinct nature of ECG content. ECG reports, often comprising brief phrases that summarize signal patterns, contrast with detailed anatomical descriptions in radiology reports. This difference in content and semantic interpretation between imaging and signal data complicates the direct application of radiology-focused methods to ECG reports. Furthermore, there is still a lack of comprehensive benchmarks for evaluating the performance of ECG report generation.

To tackle these challenges, we introduce MEIT, a **Multimodal ECG Instruction Tuning** framework that extends the capabilities of LLMs in the cardiology context to generate ECG reports using ECG signals based on human instructions. Inspired by the versatility of LLMs (Achiam et al., 2023; Touvron et al., 2023b; Wan et al., 2023b; Wang et al., 2024) in handling diverse language tasks simultaneously, we develop a specialized instruction tuning process for ECG report generation. MEIT aligns human instructions with ECG signals, enabling LLMs to generate professional-grade reports and exhibit zero-shot report generation capabilities under domain transfer scenarios across various continents and data collection devices. Specifically, leveraging publicly available ECG datasets, we construct a multimodal instruction dataset including ECG records, human instructions, and paired reports. Then, we propose an effective and efficient attention-based fusion method to integrate ECG and text representations in the latent space, enabling LLMs to understand signals for report generation without introducing additional training parameters in the attention layer.

In addition to the ECG report generation approach within

¹All data and code will be available upon acceptance.

MEIT, we introduce a comprehensive benchmark for ECG report evaluation, utilizing two datasets with 20K and 800K ECG-report pairs, respectively, across three evaluation tasks: report generation quality, zero-shot learning across datasets, and robustness analysis in the face of ECG signal perturbation. Utilizing the ECG report evaluation benchmark, we assess the proposed approach across nine open-source LLMs. The results demonstrate (1) the superior performance of MEIT in ECG report generation and the effective learning and alignment of ECG representations; (2) the effective transferability of LLMs under the MEIT framework in domain transfer scenarios.

To summarize, our primary contribution is the MELT framework, a novel approach to automating ECG report generation and evaluation based on LLMs. This framework incorporates a lightweight, attention-based fusion module effective across various LLM models. Furthermore, we establish a new benchmark for ECG report generation, which contains three aspects of the evaluation tasks. Our evaluations showcase the enhanced capabilities of instruction-tuned LLMs in generating ECG reports, highlighting the transferability in zero-shot test and robustness against data perturbations. The MEIT framework paves the way for future advances in automated ECG report generation and methodological innovations in integrating biomedical signals into LLMs.

2. Preliminaries

Electrocardiogram (ECG) measures the electrical activity of an individual’s heart over time. An ECG recording typically contains a 12-lead multivariate time series, which act as a 12-dimensional sequence of embeddings. The ECG signal offers a comprehensive view, encompassing both spatial and temporal aspects of cardiac function. ECG leads can be categorized into 6 limb leads (i.e., I, II, III, aVR, aVL, and aVF) to monitor arms and legs, providing frontal plane views, and 6 precordial leads (i.e., V1, V2, V3, V4, V5, and V6) to monitor chest, showing horizontal plane views. We denote an ECG recording as $\mathbf{X}_e \in \mathcal{R}^{M \times T}$, where M represents the numbers of leads, T is signal length. Each ECG recording is associated with an ECG report \mathbf{X}_t for description. Thus, we denote each ECG pair as $\{\mathbf{X}_e, \mathbf{X}_t\}$. More visualization details can be found in the Appendix.

3. MEIT

Figure 1 illustrates the proposed MEIT framework. We begin by describing the curation process for ECG instruction data. We then delve into the architecture of the multi-modal LLM designed for ECG report generation. Lastly, we describe the approach used to generate ECG reports with instruction tuning.

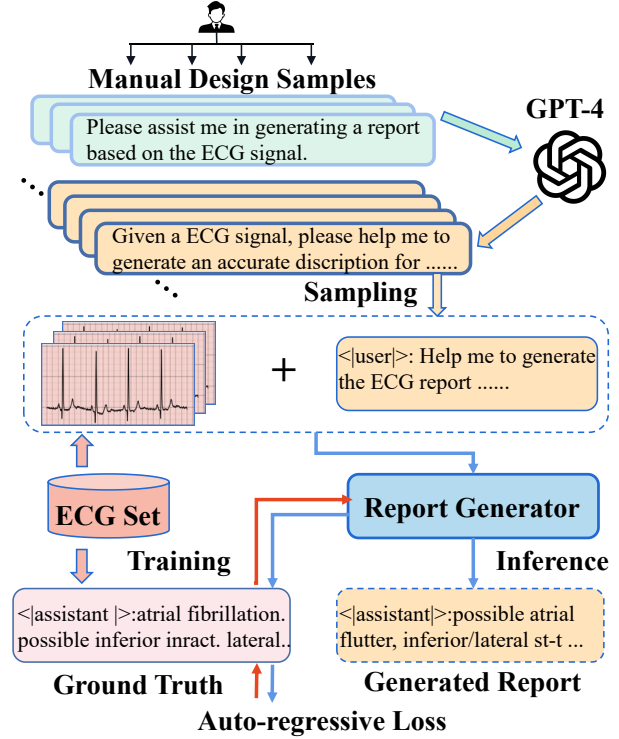


Figure 1. Illustration of the proposed MEIT framework, including ECG instruction data curation, instruction tuning on auto-regressive objective, and inference to get the generated report.

3.1. ECG Instruction Data Curation

Given an ECG signal \mathbf{X}_e , our goal during inference is to generate an ECG report using an instruction prompt. For instance, the prompt might be, “Given the ECG signal embeddings, please help me generate an accurate description for this ECG signal embeddings: ”. To achieve this goal, during the training phase, we aim to create instruction tuning data to generate a response $\hat{\mathbf{X}}_t$ that aligns semantically with the ground truth \mathbf{X}_t . In addition, since we cannot predict the exact instruction prompt that users will use, we need to ensure that our report generation process is robust enough to handle different prompts. To address this challenge, we first manually design some prompt samples, then utilize GPT-4 (Achiam et al., 2023) to generate a set of prompts by rephrasing, as shown in Figure 1. Then, we randomly select one instruction prompt \mathbf{X}_p from the prompt set, and create a general instruction-following template: $\langle \text{user} \rangle: \{\mathbf{X}_p, \mathbf{X}_e\} \langle \text{assistant} \rangle: \{\mathbf{X}_t\} \langle /s \rangle$, where $\langle \text{user} \rangle$ and $\langle \text{assistant} \rangle$ are added special tokens for tokenizer, $\langle /s \rangle$ is a stop sign for each response. This approach ensures that the generated response not only conveys the same meaning as the ground truth but also remains adaptable to different instruction prompts. Following this strategy, we construct the ECG instruction data using a MIMIC-IV-ECG (Gow et al.) dataset that contains 80K annotated data, and a 20K dataset PTB-XL (Wagner et al., 2020).

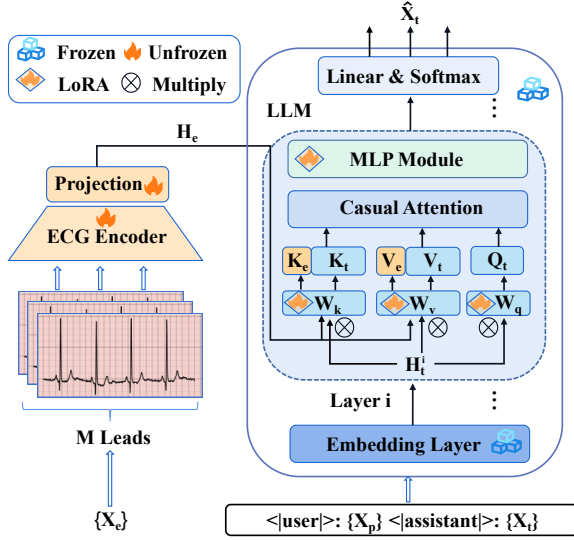


Figure 2. Illustration of model architecture for ECG report generation. \mathbf{K}_e and \mathbf{V}_e refer to linear projection of \mathbf{H}_e by multiplying shared \mathbf{W}_k and \mathbf{W}_v in the attention layer.

3.2. ECG Report Generation Model

In MEIT framework, the multimodal ECG report generation model aims to decode ECG signals end-to-end and accurately generate ECG reports. The architecture is illustrated in Figure 2. Specifically, the report generation model aims to encode the ECG-signal $\mathbf{X}_e \in \mathcal{R}^{M \times T}$ into latent embeddings and integrate them with the language embeddings with modality alignment, and then autoregressively generate the ECG report. In the following, we detail each component of the report generation model.

ECG Encoder. Since ECG signal is of high resolution in the temporal domain, it is vital to efficiently extract temporal features per lead before interaction with semantic embeddings inside the LLM backbone. Our default ECG encoder $\mathcal{F}_e(\cdot)$ consists of some temporal convolution blocks to encode each ECG signal into embeddings. Specifically, each temporal convolution block is composed of several 1-D convolution layers, batch normalization layers, and ReLU activation layers followed by average pooling. To align the output dimension with the head dimension of LLM backbone $\mathcal{F}_l(\cdot)$, we employ a non-linear up-to-down projection layer $\mathcal{P}_e(\cdot)$ to obtain the ECG embeddings:

$$\mathbf{H}_e = \mathcal{P}_e(\mathcal{F}_e(\mathbf{X}_e)), \quad (1)$$

where $\mathbf{H}_e \in \mathcal{R}^{D_h}$, D_h has the same dimension as the multi-head attention layers of LLMs. Note that our default ECG encoder is lightweight and is able to learn temporal patterns of signals without a long training period.

ECG Modality Alignment. To guide the LLMs in aligning ECG signal data with corresponding textual outputs, we introduce an ECG modality alignment strategy. This approach

is detailed in Figure 2. Specifically, given the ECG embeddings \mathbf{Z}_e , the alignment strategy aims to incorporate \mathbf{Z}_e with the current hidden state \mathbf{H}_t^i generated from previous $i - 1$ -th layer of the LLM backbone $\mathcal{F}_l(\cdot)$ for next-token prediction task. Here \mathbf{H}_t^i is defined as:

$$\mathbf{H}_t^i = \mathcal{F}_l^{i-1}([\mathbf{X}_p, \mathbf{X}_t]), \quad (2)$$

where i is the current layer index. Different from gated-attention fusion in Flamingo (Alayrac et al., 2022), Memorizing Transformer (Wu et al., 2022), and G-MAP (Wan et al., 2022), or Q-former in BLIP-2 (Li et al., 2023a) that require the additional trainable parameters or design complex modules, we propose a simple yet effective concatenated-fusion method that directly injects the ECG embeddings with language context in the causal-attention (C-Attn) of the models. In our approach, each attention layer combines \mathbf{H}_e , generated from the ECG encoder and projector as a prefix condition, with \mathbf{H}_t^i , derived from the preceding layer. The fusion process is as follows:

$$\text{C-Attn}(\mathbf{H}_e, \mathbf{H}_t^i) = [\text{head}_1, \dots, \text{head}_k] \mathbf{W}_o, \quad (3)$$

here, k represents the number of attention heads, and \mathbf{W}_o , a matrix in $\mathcal{R}^{kD_h \times D_m}$, serves as the projection matrix with D_m denoting the hidden size of the LLM backbone. We replicate \mathbf{H}_e for each head k times, merging the ECG and language features in the sequence dimension. This is achieved through a shared projection of keys and values for each pattern. The fusion is then articulated as:

$$\mathbf{K}_{m,j} = [\mathbf{K}_{e,j}, \mathbf{K}_{t,j}]^\top, \mathbf{V}_{m,j} = [\mathbf{V}_{e,j}, \mathbf{V}_{t,j}], \quad (4)$$

$$\text{head}_j = \text{Softmax}\left(\frac{\mathbf{Q}_{t,j} \mathbf{K}_{m,j}}{\sqrt{D_h}}\right) \mathbf{V}_{m,j}, \quad (5)$$

where $\mathbf{Q}_{t,j} = \mathbf{H}_{t,j}^i \mathbf{W}_{q,j}$, $\mathbf{K}_{e,j} = \mathbf{H}_e \mathbf{W}_{k,j}$, and $\mathbf{K}_{t,j} = \mathbf{H}_{t,j}^i \mathbf{W}_{k,j}$, with a similar notation for $\mathbf{V}_{e,j} = \mathbf{H}_e \mathbf{W}_{v,j}$ and $\mathbf{V}_{t,j} = \mathbf{H}_{t,j}^i \mathbf{W}_{v,j}$. Concatenation is denoted by $[\cdot]$, and $\mathbf{K}_{m,j}$ and $\mathbf{V}_{m,j}$ symbolize the amalgamated features of query and key. $\mathbf{W}_{q,j}$, $\mathbf{W}_{k,j}$, and $\mathbf{W}_{v,j}$ in $\mathcal{R}^{D_h \times D_h}$ represent the projection matrices for query, key, and value for each head j , respectively. Our model’s design allows for the efficient fusion of two modalities through causal attention, facilitating conditional generation without the need for additional parameter updates to align the ECG modality.

3.3. ECG Instruction Tuning

As described in Section 3.1, we have converted ECG-text pairs into a chat-bot style instruction format: $\langle \text{user} \rangle: \{\mathbf{X}_p, \mathbf{X}_e\} \langle \text{assistant} \rangle: \{\mathbf{X}_t\} \langle \text{s} \rangle$. During instruction tuning, we compute autoregressive loss only on tokens after response tokens $\langle \text{assistant} \rangle$, and use label loss

masking to finetune the model, where we mask all tokens belonging to \mathbf{X}_p and \mathbf{X}_e . To save computational resources and accelerate the convergence of instruction tuning, we use the LoRA (Hu et al., 2021) adapters for all linear layers of the LLM backbone \mathcal{F}_l and freeze its backbone. Subsequently, given a sequence of ECG instruction data, we compute the probability of the target response \mathbf{X}_t as an autoregressive function:

$$p(\mathbf{X}_t | \mathbf{X}_p, \mathbf{X}_e) = \prod_{i=j}^L p_{\theta}(\mathbf{x}_{t,i} | \mathbf{X}_p, \mathbf{X}_e, \mathbf{X}_{t,<i}), \quad (6)$$

where j is the start index after `<assistant>`, θ is the trainable parameters of LoRA and ECG encoder \mathcal{F}_e , $\mathbf{X}_{t,<i}$ is the response tokens before the current generation $\mathbf{x}_{t,i}$.

4. Benchmarking ECG Report Generation

In this section, we create a benchmark to evaluate the ECG report generation approach. Our benchmark includes two datasets (PTB-XL and MIMIC-IV-ECG) along with three ECG-related tasks, including (1) the quality of ECG report generation; (2) the zero-shot ability under domain transfer; (3) the robustness of model against perturbed signals.

4.1. Datasets

PTB-XL. The PTB-XL dataset (Wagner et al., 2020) comprises 21,837 clinical 12-lead ECGs, each lasting 10 seconds, from 18,885 patients. Each ECG is accompanied by a corresponding report. The data includes raw ECG signals and their reports, with all recordings sampled at 500Hz over 10 seconds. We divided this dataset into training, validation, and testing subsets in a 70%:10%:20% ratio, respectively. The human experts double-check all samples in the test set to ensure data quality. We reformulate the dataset into instruction data format as mentioned in Sec 2.

MIMIC-IV-ECG. The MIMIC-IV-ECG dataset (Gow et al.) is currently the largest publicly accessible ECG dataset, containing 800,035 paired samples from 161,352 unique subjects. Similar to PTB-XL, each sample in this dataset includes a raw ECG signal and its corresponding report, with all recordings sampled at 500Hz for 10 seconds. The division of this dataset into training, validation, and testing subsets is 80%:10%:10% ratio. Likewise, we reconstruct this dataset into an ECG instruction data template.

4.2. Evaluation Metrics

We evaluate models using nine metrics: BLEU 1-4 (Papineni et al., 2002), METEOR (Banerjee & Lavie, 2005), ROUGE 1-2 and L (Lin, 2004), CIDEr-D (Vedantam et al., 2015), and BERTScore (Zhang et al., 2019). BLEU and METEOR assess the quality of machine translation, focusing on accuracy and fluency. ROUGE-L measures sentence

fluency and structure, while ROUGE-1 and ROUGE-2 examine uni-gram and bi-gram overlaps. CIDEr-D evaluates the relevance and uniqueness of generated ECG reports against a candidate set, and BERTScore assesses semantic similarity to the ground truth, ensuring content accuracy.

4.3. Tasks

We evaluate the performance of ECG report generation on the following three tasks:

Quality Report Generation. The goal of this task is to evaluate the quality of report generation following ECG instruction tuning. We utilize 10% of the MIMIC-IV-ECG and PTB-XL datasets, designated for instruction tuning, as the test set. This evaluation focuses on the syntactic and semantic similarities between the generated ECG report and the ground truth, based on diverse instructions and input ECG signals. For task assessment, we employ BLEU-1 to 4, METEOR, ROUGE 1, 2, and L, CIDEr-D, and BERTScore.

Zero-shot Generalizability. To explore the generalizability of LLMs in domain transfer scenarios following ECG instruction tuning, we trained the models on 70% of the instruction data from MIMIC-IV-ECG. We then assessed the zero-shot capabilities of these models on the PTB-XL test set, which contains high-quality ground truth evaluated by clinical experts. For model evaluation, we used the metrics BLEU-3, BLEU-4, METEOR, and ROUGE-L and calculated their average.

Signal Perturbation Robustness. In real-world clinical settings, ECG signals often contain some degree of noise. To evaluate the robustness of MEIT against such noisy interference, we selected 10% of the ECG samples from the MIMIC-IV-ECG test dataset. We then added Gaussian noise to these samples during the models’ instruction-based inference process. For this evaluation, we used BLEU-4, METEOR, ROUGE-L, and CIDEr-D as metrics.

5. Experiments and Evaluation

In this section, we evaluate and benchmark nine open-source decoder-only LLMs using the constructed ECG report generation benchmark. Additionally, we offer a comprehensive analysis of scalability and instruction tuning and present case studies showcasing the generated reports.

5.1. Experimental Settings

Models. We use nine LLMs based on the `peft`² library, which directly supports the LoRA (Hu et al., 2021) module, to construct the multimodal ECG report generation model described in Section 3.2. These models include GPT-

²<https://github.com/huggingface/peft>

Electrocardiogram Instruction Tuning for Report Generation

Table 1. Natural language generation metric on MIMIC-IV-ECG. For model size, 'M' denotes the million level, and 'B' denotes the billion level. † refers to an improved instruct fine-tuned version of models. The light teal color indicates the second highest results, and heavy teal color indicates the highest results.

| MODELS | SIZE | BLEU-1 | BLEU-2 | BLEU-3 | BLEU-4 | METEOR | ROUGE-L | ROUGE-1 | ROUGE-2 | CIDEr-D |
|-------------------|------|--------|--------|--------|--------|--------|---------|---------|---------|---------|
| GPT2-Medium | 345M | 0.576 | 0.527 | 0.456 | 0.425 | 0.551 | 0.523 | 0.544 | 0.512 | 3.70 |
| GPT2-Large | 774M | 0.614 | 0.563 | 0.490 | 0.476 | 0.595 | 0.571 | 0.585 | 0.538 | 4.21 |
| GPT-Neo | 2.7B | 0.631 | 0.579 | 0.534 | 0.489 | 0.727 | 0.689 | 0.715 | 0.592 | 4.81 |
| GPT-NeoX | 20B | 0.645 | 0.588 | 0.539 | 0.523 | 0.719 | 0.701 | 0.712 | 0.622 | 4.92 |
| GPT-J | 6B | 0.676 | 0.628 | 0.584 | 0.542 | 0.756 | 0.721 | 0.744 | 0.632 | 5.23 |
| BLOOM | 7B | 0.669 | 0.624 | 0.591 | 0.550 | 0.758 | 0.725 | 0.745 | 0.639 | 5.19 |
| OPT | 6.7B | 0.673 | 0.616 | 0.598 | 0.532 | 0.755 | 0.732 | 0.743 | 0.631 | 5.32 |
| LLaMA-1 | 7B | 0.685 | 0.648 | 0.615 | 0.543 | 0.761 | 0.724 | 0.742 | 0.642 | 5.26 |
| Mistral | 7B | 0.697 | 0.659 | 0.611 | 0.571 | 0.763 | 0.740 | 0.765 | 0.658 | 5.48 |
| LLaMA-2† | 7B | 0.706 | 0.662 | 0.622 | 0.581 | 0.775 | 0.745 | 0.768 | 0.664 | 5.55 |
| Mistral-Instruct† | 7B | 0.714 | 0.665 | 0.619 | 0.576 | 0.768 | 0.751 | 0.762 | 0.667 | 5.62 |

Table 2. Natural language generation metric on PTB-XL. The light teal color indicates the second highest results, and heavy teal color indicates the highest results.

| MODELS | SIZE | BLEU-1 | BLEU-2 | BLEU-3 | BLEU-4 | METEOR | ROUGE-L | ROUGE-1 | ROUGE-2 | CIDEr-D |
|-------------------|------|--------|--------|--------|--------|--------|---------|---------|---------|---------|
| GPT2-Medium | 345M | 0.329 | 0.278 | 0.254 | 0.232 | 0.441 | 0.391 | 0.561 | 0.433 | 2.12 |
| GPT2-Large | 774M | 0.437 | 0.395 | 0.355 | 0.320 | 0.575 | 0.481 | 0.652 | 0.527 | 3.25 |
| GPT-Neo | 2.7B | 0.474 | 0.449 | 0.398 | 0.373 | 0.602 | 0.486 | 0.674 | 0.595 | 3.70 |
| GPT-NeoX | 20B | 0.469 | 0.453 | 0.417 | 0.399 | 0.620 | 0.553 | 0.688 | 0.622 | 3.58 |
| GPT-J | 6B | 0.485 | 0.452 | 0.428 | 0.405 | 0.656 | 0.550 | 0.662 | 0.613 | 3.72 |
| BLOOM | 7B | 0.491 | 0.462 | 0.427 | 0.415 | 0.665 | 0.580 | 0.678 | 0.605 | 3.80 |
| OPT | 6.7B | 0.502 | 0.477 | 0.431 | 0.418 | 0.662 | 0.568 | 0.669 | 0.624 | 3.94 |
| LLaMA-1 | 7B | 0.514 | 0.485 | 0.465 | 0.430 | 0.678 | 0.588 | 0.682 | 0.613 | 3.97 |
| Mistral | 7B | 0.486 | 0.475 | 0.446 | 0.421 | 0.673 | 0.591 | 0.697 | 0.634 | 3.98 |
| LLaMA-2† | 7B | 0.515 | 0.484 | 0.469 | 0.439 | 0.675 | 0.594 | 0.698 | 0.624 | 4.05 |
| Mistral-Instruct† | 7B | 0.501 | 0.481 | 0.457 | 0.425 | 0.664 | 0.592 | 0.700 | 0.641 | 4.01 |

Table 3. Semantic similarity between the generated ECG reports and ground truths is measured using BERTScore, denoted as P for Precision, R for Recall, and F-1 for the F-1 Score.

| MODELS | MIMIC-IV-ECG | | | PTB-XL | | |
|-------------------|--------------|-------|-------|--------|-------|-------|
| | P | R | F-1 | P | R | F-1 |
| GPT2-Medium | 0.562 | 0.453 | 0.502 | 0.534 | 0.465 | 0.497 |
| GPT2-Large | 0.657 | 0.574 | 0.613 | 0.625 | 0.553 | 0.586 |
| GPT-Neo | 0.723 | 0.633 | 0.675 | 0.675 | 0.588 | 0.628 |
| GPT-NeoX | 0.719 | 0.638 | 0.676 | 0.654 | 0.579 | 0.614 |
| GPT-J | 0.725 | 0.655 | 0.688 | 0.689 | 0.622 | 0.654 |
| BLOOM | 0.734 | 0.684 | 0.708 | 0.701 | 0.645 | 0.672 |
| OPT | 0.713 | 0.667 | 0.689 | 0.712 | 0.648 | 0.678 |
| LLaMA-1 | 0.752 | 0.697 | 0.723 | 0.725 | 0.657 | 0.689 |
| Mistral | 0.761 | 0.732 | 0.746 | 0.711 | 0.664 | 0.687 |
| LLaMA-2† | 0.764 | 0.725 | 0.744 | 0.721 | 0.668 | 0.693 |
| Mistral-Instruct† | 0.773 | 0.722 | 0.747 | 0.730 | 0.661 | 0.694 |

Neo (Black et al., 2021), GPT-NeoX (Black et al., 2022), GPT-J (Wang & Komatsuzaki, 2021), BLOOM (Workshop et al., 2022), OPT (Zhang et al., 2022), LLaMA-1 (Touvron et al., 2023a), LLaMA-2 (Touvron et al., 2023b), Mis-

tral (Jiang et al., 2023), and Mistral-Instruct³, along with two relatively small pre-trained language models (GPT2-Medium and GPT-Large (Radford et al., 2019)) as fundamental baselines.

Implementation Details. Our experiment is implemented using PyTorch 2.1, the latest transformers (Wolf et al., 2020), and the accelerate (Gugger et al., 2022) library on $4 \times A100$ GPUs. We utilize the official weights for all LLMs from Hugging Face (Wolf et al., 2019) for evaluation, with sizes ranging from 2.7 billion to 70 billion parameters. For models exceeding 10 billion parameters, we use DeepSpeed⁴ for training. All models are trained on both MIMIC-IV-ECG and PTB-XL instruction datasets for 5 epochs with a learning rate of $2e-5$ and a batch size of 64. We adopt a linear optimizer scheduler with a warm-up ratio of 0.03. The best performance of each model is determined by training on the training set, selecting from the validation set, and evaluating on the test set. More details about instruction tuning can be

³<https://huggingface.co/mistralai/Mistral-7B-Instruct-v0.1>

⁴<https://github.com/microsoft/DeepSpeed>

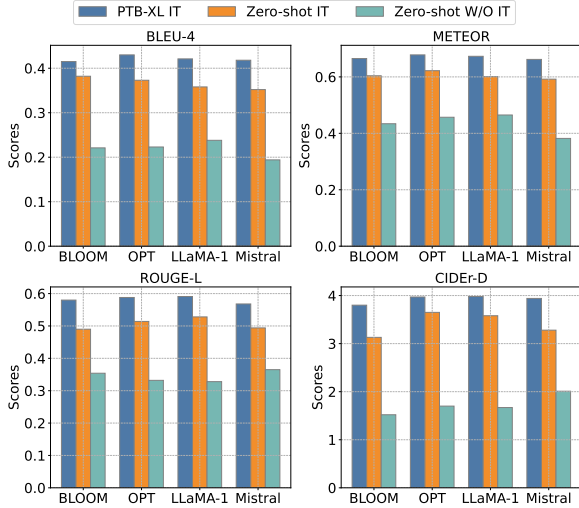


Figure 3. Zero-shot performance on PTB-XL dataset. “IT” denotes instruction tuning.

found in the appendix.

5.2. Benchmark Task Evaluation

5.2.1. QUALITY EVALUATION

Performance on MIMIC-IV-ECG. Table 1 and 3 present the results of various types of language encoders $\mathcal{F}_l(\cdot)$ on MIMIC-IV-ECG. The results show that all LLMs exhibit superior performance compared to smaller language models (SLMs), such as GPT2-Medium and GPT2-Large, across all evaluation metrics. Notably, from GPT-Neo to Mistral-Instruct, LLM-based backbones achieve a significant margin over SLMs in all metrics. For instance, compared to GPT2-Large, the METEOR score increases in the range of 0.132 to 0.18 from GPT-Neo to LLaMA-2, and Mistral-Instruct outperforms GPT2-Large with an improvement of 0.18 in the ROUGE-L score and 0.134 in the F-1 of BERTScore.

The observed performance underscores the adeptness of LLMs in generalizing from signal data, showcasing enhanced proficiency in aligning ECG signal representations with corresponding textual information. This highlights the significant potential of LLMs in the domain of medical signal-to-text generation. Particularly, LLaMA-2 and Mistral-Instruct surpass their counterparts in the majority of evaluative metrics, suggesting that models pre-tuned with general instructions are more adept at learning ECG-text alignment.

Performance on PTB-XL. As shown in Table 2, the models exhibit reduced performance on PTB-XL compared to MIMIC-IV-ECG, which is attributable to the smaller scale of the instruction data in PTB-XL. This underscores the importance of data scale in enhancing instruction-based ECG report generation. Moreover, similar to the MIMIC-

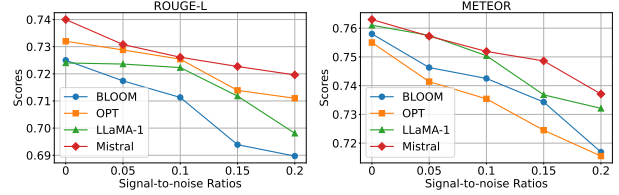


Figure 4. Signal perturbation robustness analysis on various LLMs

IV-ECG results, all LLM-based models show significant improvement over SLMs. Specifically, LLaMA-2 surpasses GPT2-Large by 0.134 in the BLEU-3 metric, while LLaMA-1 achieves a 0.103 improvement in the METEOR score. The overall experimental results reveal that Mistral-Instruct and LLaMA-2 are consistently the top two performers across most metrics, because of their strong general instruction-following capabilities. Consequently, we select LLaMA-2 and Mistral-Instruct as the default architectures for our framework.

5.2.2. ZERO-SHOT EVALUATION IN DOMAIN TRANSFER.

In Figure 3, we present the evaluation of the zero-shot learning capabilities of various LLMs, which is trained on the MIMIC-IV-ECG dataset and then tested on PTB-XL (unseen dataset). The assessed models include BLOOM, OPT, LLaMA-1, and Mistral. Firstly, all selected LLMs undergo instruction tuning on the MIMIC-IV-ECG train set, followed by zero-shot testing on the PTB-XL test set verified by human experts, denoted as ZERO-SHOT IT. We also measure the performance of each model in report generation without prior ECG-specific instruction tuning, denoted as ZERO-SHOT W/O IT. PTB-XL IT represents training on the PTB-XL train set and then evaluated on the PTB-XL test set. Notably, although ZERO-SHOT IT shows a slight degradation compared to PTB-XL IT, the results still indicate a variance in the models’ ability to generalize to an unseen dataset with instruction tuning (IT), compared to ZERO-SHOT W/O IT. The involvement of ECG instruction tuning on MIMIC-IV-ECG enables the models to achieve superior zero-shot performance on the unseen PTB-XL dataset, indicating the necessity of instruction tuning in enhancing the models’ zero-shot ability on unseen datasets in ECG report generation.

5.2.3. ROBUST ANALYSIS WITH PERTURBED ECG SIGNAL.

In a noise stress evaluation (Wang et al., 2019), we added Gaussian noise to ECG signals at signal-to-noise ratios (SNRs) of 0.05, 0.1, 0.15, and 0.2 during testing to assess model robustness. Our experiments utilized four LLM architectures: BLOOM, OPT, LLaMA-1, and Mistral, each trained on clean ECG signals from the MIMIC-IV-ECG

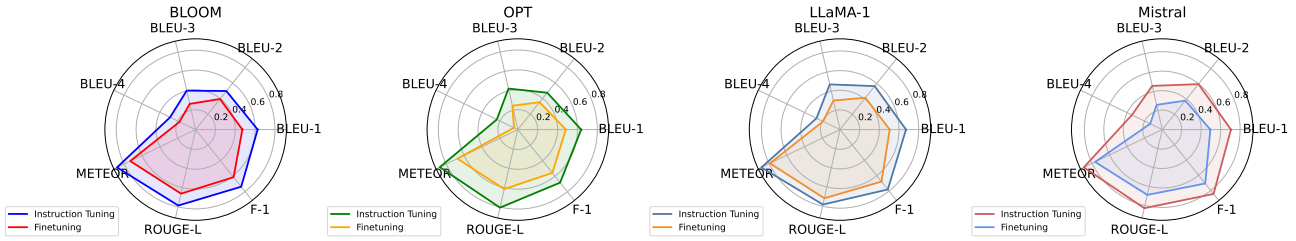


Figure 5. Ablation Study of ECG Instruction Tuning on MIMIC-IV-ECG Dataset.

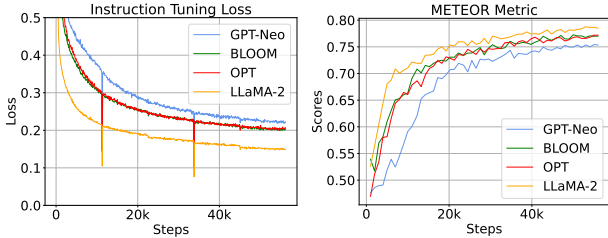


Figure 6. Instruction tuning loss and METEOR visualization.

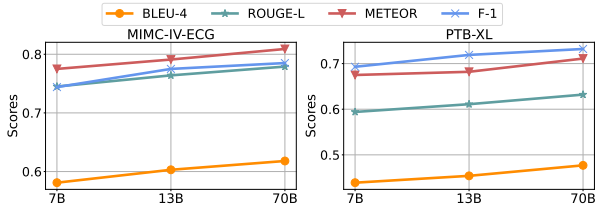


Figure 7. Model Scaling Performance on MIMIC-IV-ECG and PTB-XL.

training set and tested on corresponding noise-added signals from its test set. The results, illustrated in Figure 4, show a performance decline in all LLMs as SNR increased, highlighting the significant interference of ECG noise. Furthermore, as shown in Table 1, Mistral also excelled in tests on noise-free datasets, suggesting a synergistic effect between clean and noisy test sets. The results demonstrate Mistral’s strong resistance to perturbations. Even with more severe noise, it maintained robustness in terms of ROUGE-L and METEOR metrics. Developing an even more robust framework is a goal for future research.

5.3. Analysis

5.3.1. INSTRUCTION TUNING VISUALIZATION.

Figure 6 compares the convergence curves of the instruction tuning loss and the METEOR score between GPT-Neo (2.7B), BLOOM (7B), OPT (6.7B), and LLaMA-2 (7B) on the MIMIC-IV-ECG train and validation datasets. We observe that larger models with more parameters can converge to a smaller loss and achieve higher performance on the METEOR score. Notably, an increase in model size correlates with higher performance and lower loss, suggesting that larger models have the potential for better performance.

5.3.2. SCALABILITY ANALYSIS.

To investigate whether ECG instruction tuning on larger-scale models yields better results, we validated LLaMA-2 models of 7B and 13B parameter sizes on both MIMIC-IV-ECG and PTB-XL datasets. As depicted in 7, an upward trend in all evaluation metrics is observed with a gradual increase in model size. However, it is noteworthy that the gains in performance associated with increasing model size are not particularly significant. For example, the F-1 score for the 70B model on the PTB-XL dataset exhibits a marginal increase of 0.02 over the 13B model. Similarly, on the MIMIC-IV-ECG dataset, the 70B model’s F-1 score is only 0.01 higher than that of the 13B model. Therefore, we conjecture that enhancing both data scale and model size concurrently is necessary to achieve superior performance (Wei et al., 2022).

5.3.3. ABLATION STUDY ON ECG INSTRUCTION TUNING.

To validate the effectiveness of adopting an instruction tuning paradigm for aligning ECG signals and report representations, we conducted the following ablation experiment. We selected BLOOM, OPT, LLaMA-1, and Mistral as LLM backbones and removed the instruction tuning strategy, allowing the language models to fine-tune directly in the setting of generating text from ECG signals only. As shown in Figure 5, aligning ECG and report representations using direct fine-tuning, as opposed to instruction tuning, results in a significant decline across all metrics. Particularly in the Mistral model, the instruction tuning paradigm notably outperforms direct fine-tuning. These results demonstrate that, compared to fine-tuning, instruction tuning more effectively enhances the generalization ability of LLMs on unseen tasks/data (Ouyang et al., 2022).

5.3.4. QUALITATIVE RESULTS.

In Figure 8, we randomly select two samples generated by MEIT using LLaMA-2 and Mistral-Instruct as the LLM backbones. The consistent key information, highlighted in blue, indicates that both models have successfully learned important patterns from the ECG signals. Overall, the mod-

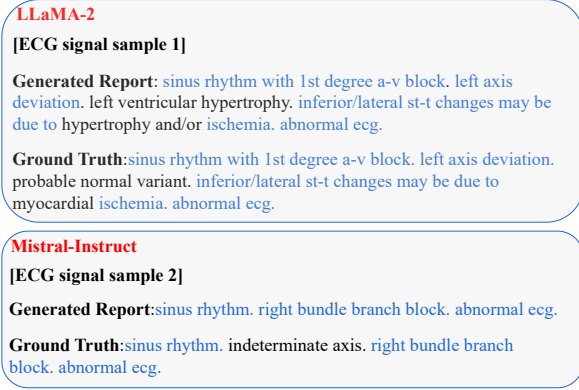


Figure 8. Examples of ECG reports generated by LLaMA-2 and Mistral-Instruct. We highlight the consistent information between the generated reports and the ground truths with blue color.

els’ results align with the ground truth, accurately identifying cardiac abnormalities from the ECG signals. Furthermore, both models provide detailed explanations of abnormal ECG signal details, such as ‘ischemia’ from sample 1 and ‘right bundle branch block’ from sample 2. These generated reports demonstrate the efficacy of our method.

6. Related Work

Instruction Tuning. Instruction tuning (Zhang et al., 2023a; Wang et al., 2023) is designed to enhance the zero-shot capabilities of LLMs on new tasks using either machine-generated or human-annotated instructions. Notable examples such as InstructGPT (Ouyang et al., 2022), FLAN-PaLM (Chung et al., 2022), and Alpaca (Taori et al., 2023) utilize various methods, including manual collection and human feedback, to generate instruction template data for fine-tuning. In the realm of multimodal learning, models like LLaVA (Liu et al., 2023b), MiniGPT-4 (Zhu et al., 2023), and AnyMAL (Moon et al., 2023) demonstrate the utility of multimodal instruction data to enhance learning across different modalities. However, medical signals such as ECG and their corresponding text remain underexplored. Our work bridges this gap by developing a specialized ECG-related instruction tuning framework, thereby improving the generation of ECG reports.

Medical Report Generation. Different from medical vision-language alignment (Wan et al., 2023a), medical Report Generation can be categorized into three main approaches: (1) Template Selection and Generation, where methods like HRGR (Li et al., 2018) focus on sentence creation or template retrieval, and CMAS (Jing et al., 2017) uses dual writers for differentiating regions; (2) Data Integration and Coherence, illustrated by PPKED’s (Liu et al., 2021b) knowledge merging for consistency, and CA’s contrasting of abnormal features (Ma et al., 2021); (3) Cross-Modal Alignment, with (Chen et al., 2022b; Qin & Song,

2022) using attention mechanisms for text-visual feature correlation. Recent advancements (Gu et al., 2024; Tanida et al., 2023; Li et al., 2023c) focus on local visual feature learning and multi-level cross-modal alignment, showcasing the evolution of semantic matching in radiology report generation. However, these approaches mainly focus on radiology report generation, directly applying these approaches to ECG data is challenging because the patterns between medical images and ECG biomedical signals are significantly different.

Signal-to-Text Generation. Signal-to-Text (S2T) generation, predominantly speech-to-text, converts speech signals into text. Extensive research (Baeovski et al., 2020; Chen et al., 2020; Liu et al., 2021a; Zheng et al., 2021; Hsu et al., 2021; Bapna et al., 2021) has extensively studied patterns in speech signals, analyzing both temporal and spectral aspects. Although the field of ECG report generation is largely unexplored, the use of speech signal research techniques in the creation of ECG reports presents significant challenges due to fundamental differences: (1) Speech signals for S2T tasks typically have a sampling frequency of up to 16,000 - 60,000 Hz (Lavry, 2012; Painter & Spanias, 2000; Byrne et al., 1994) and are monochannel, while ECG signals usually have a lower sampling frequency of around 500 Hz and encompass 12 channels. (2) Speech signals can be discretized into acoustic units corresponding to specific words (Défossez et al., 2022), but ECG signals lack such discrete units. Certain cardiac conditions, like bundle branch block, can obscure or distort the heartbeats patterns in ECG readings. (3) Speech signals and their transcriptions maintain strong temporal alignment, as each word correlates with a specific acoustic pattern, and the transcription follows the temporal sequence of speech (Zhang et al., 2023b). In contrast, ECG reports evaluate the cardiac patterns on a global level, assessing the entire ECG period rather than focusing on individual acoustic-like units in speech. These fundamental differences between speech-text pairs and ECG records, in both signal and text terms, highlight the need for S2T methods specifically designed for ECG data. Furthermore, the scarcity of research in the generation of ECG reports highlights an urgent need for comprehensive benchmarks using large-scale, publicly accessible data sets.

7. Conclusion and Future Work

In this work, we propose and demonstrate the efficacy of the Multimodal ECG Instruction Tuning (MEIT) framework. Particularly, we first introduce a novel method for creating instruction-following data for ECG reports, enabling the training of an ECG report generator, a multimodal LLM designed to generate ECG reports following human instructions. Furthermore, we propose an effective and efficient method for aligning ECG and report representations across multiple open-source LLMs, achieving notable performance

on both the MIMIC-IV-ECG and PTB-XL datasets for diverse tasks. Importantly, this paper introduces the comprehensive benchmark for ECG instruction-following in ECG report generation. While this research primarily concentrates on ECG signals, it marks a preliminary step in biomedical signal instruction tuning. In future work, we plan to extend our framework to encompass additional medical signal domains, such as EEG signals, with the aspiration that our work spurs further advancements in developing more proficient medical-signal LLMs.

Broader Impact

Our MEIT framework first attempt to addresses automatic ECG report generation through ECG instruction tuning, establishing the first comprehensive benchmark for this process with mainstream LLMs. In this work, we mainly focus on generating reports from multimodal ECG instructions using LLMs. However, the generated results are not fully explainable or controllable, even though the generation procedure is transparent and trackable. This is because the underlying theory of LLMs remains largely unexplored, necessitating further investigation to ensure the quality and safety of the generated content. In the future, we aim to enable LLMs to utilize external, expert-verified knowledge databases, such as clinical protocols and medical textbooks, to enhance the explainability of the generated ECG reports.

References

- Achiam, J., Adler, S., Agarwal, S., Ahmad, L., Akkaya, I., Aleman, F. L., Almeida, D., Altenschmidt, J., Altman, S., Anadkat, S., et al. Gpt-4 technical report. *arXiv preprint arXiv:2303.08774*, 2023.
- Alayrac, J.-B., Donahue, J., Luc, P., Miech, A., Barr, I., Hasson, Y., Lenc, K., Mensch, A., Millican, K., Reynolds, M., et al. Flamingo: a visual language model for few-shot learning. *Advances in Neural Information Processing Systems*, 35:23716–23736, 2022.
- Baevski, A., Zhou, Y., Mohamed, A., and Auli, M. wav2vec 2.0: A framework for self-supervised learning of speech representations. *Advances in neural information processing systems*, 33:12449–12460, 2020.
- Banerjee, S. and Lavie, A. Meteor: An automatic metric for mt evaluation with improved correlation with human judgments. In *Proceedings of the acl workshop on intrinsic and extrinsic evaluation measures for machine translation and/or summarization*, pp. 65–72, 2005.
- Bapna, A., Chung, Y.-a., Wu, N., Gulati, A., Jia, Y., Clark, J. H., Johnson, M., Riesa, J., Conneau, A., and Zhang, Y. Slam: A unified encoder for speech and language modeling via speech-text joint pre-training. *arXiv preprint arXiv:2110.10329*, 2021.
- Black, S., Gao, L., Wang, P., Leahy, C., and Biderman, S. GPT-Neo: Large Scale Autoregressive Language Modeling with Mesh-Tensorflow, March 2021. URL <https://doi.org/10.5281/zenodo.5297715>. If you use this software, please cite it using these metadata.
- Black, S., Biderman, S., Hallahan, E., Anthony, Q., Gao, L., Golding, L., He, H., Leahy, C., McDonell, K., Phang, J., et al. Gpt-neox-20b: An open-source autoregressive language model. *arXiv preprint arXiv:2204.06745*, 2022.
- Byrne, D., Dillon, H., Tran, K., Arlinger, S., Wilbraham, K., Cox, R., Hagerman, B., Hetu, R., Kei, J., Lui, C., et al. An international comparison of long-term average speech spectra. *The journal of the acoustical society of America*, 96(4):2108–2120, 1994.
- Chen, J., Ma, M., Zheng, R., and Huang, L. Mam: Masked acoustic modeling for end-to-end speech-to-text translation. *arXiv preprint arXiv:2010.11445*, 2020.
- Chen, J., Liao, K., Wei, K., Ying, H., Chen, D. Z., and Wu, J. Me-gan: Learning panoptic electrocardio representations for multi-view ecg synthesis conditioned on heart diseases. In *International Conference on Machine Learning*, pp. 3360–3370. PMLR, 2022a.
- Chen, Z., Shen, Y., Song, Y., and Wan, X. Cross-modal memory networks for radiology report generation. *arXiv preprint arXiv:2204.13258*, 2022b.
- Chung, H. W., Hou, L., Longpre, S., Zoph, B., Tay, Y., Fedus, W., Li, Y., Wang, X., Dehghani, M., Brahma, S., et al. Scaling instruction-finetuned language models. *arXiv preprint arXiv:2210.11416*, 2022.
- Défossez, A., Copet, J., Synnaeve, G., and Adi, Y. High fidelity neural audio compression. *arXiv preprint arXiv:2210.13438*, 2022.
- Gow, B., Pollard, T., Nathanson, L. A., Johnson, A., Moody, B., Fernandes, C., Greenbaum, N., Berkowitz, S., Moukheiber, D., Eslami, P., et al. Mimir-iv-ecg-diagnostic electrocardiogram matched subset.
- Gu, T., Liu, D., Li, Z., and Cai, W. Complex organ mask guided radiology report generation. In *Proceedings of the IEEE/CVF Winter Conference on Applications of Computer Vision*, pp. 7995–8004, 2024.
- Gugger, S., Debut, L., Wolf, T., Schmid, P., Mueller, Z., Mangrulkar, S., Sun, M., and Bossan, B. Accelerate: Training and inference at scale made simple, efficient and adaptable. <https://github.com/huggingface/accelerate>, 2022.

- Hsu, W.-N., Bolte, B., Tsai, Y.-H. H., Lakhotia, K., Salakhutdinov, R., and Mohamed, A. Hubert: Self-supervised speech representation learning by masked prediction of hidden units. *IEEE/ACM Transactions on Audio, Speech, and Language Processing*, 29:3451–3460, 2021.
- Hu, E. J., Wallis, P., Allen-Zhu, Z., Li, Y., Wang, S., Wang, L., Chen, W., et al. Lora: Low-rank adaptation of large language models. In *International Conference on Learning Representations*, 2021.
- Hu, R., Chen, J., and Zhou, L. Spatiotemporal self-supervised representation learning from multi-lead ecg signals. *Biomedical Signal Processing and Control*, 84: 104772, 2023.
- Jiang, A. Q., Sablayrolles, A., Mensch, A., Bamford, C., Chaplot, D. S., Casas, D. d. l., Bressand, F., Lengyel, G., Lample, G., Saulnier, L., et al. Mistral 7b. *arXiv preprint arXiv:2310.06825*, 2023.
- Jing, B., Xie, P., and Xing, E. On the automatic generation of medical imaging reports. *arXiv preprint arXiv:1711.08195*, 2017.
- Langley, P. Crafting papers on machine learning. In Langley, P. (ed.), *Proceedings of the 17th International Conference on Machine Learning (ICML 2000)*, pp. 1207–1216, Stanford, CA, 2000. Morgan Kaufmann.
- Lavry, D. The optimal sample rate for quality audio. *Lavry Engineering Inc*, 2012.
- Li, J., Li, D., Savarese, S., and Hoi, S. Blip-2: Bootstrapping language-image pre-training with frozen image encoders and large language models. *arXiv preprint arXiv:2301.12597*, 2023a.
- Li, J., Liu, C., Cheng, S., Arcucci, R., and Hong, S. Frozen language model helps ecg zero-shot learning. *arXiv preprint arXiv:2303.12311*, 2023b.
- Li, Y., Liang, X., Hu, Z., and Xing, E. P. Hybrid retrieval-generation reinforced agent for medical image report generation. *Advances in neural information processing systems*, 31, 2018.
- Li, Y., Yang, B., Cheng, X., Zhu, Z., Li, H., and Zou, Y. Unify, align and refine: Multi-level semantic alignment for radiology report generation. In *Proceedings of the IEEE/CVF International Conference on Computer Vision*, pp. 2863–2874, 2023c.
- Lin, C.-Y. Rouge: A package for automatic evaluation of summaries. In *Text summarization branches out*, pp. 74–81, 2004.
- Liu, A. T., Li, S.-W., and Lee, H.-y. Tera: Self-supervised learning of transformer encoder representation for speech. *IEEE/ACM Transactions on Audio, Speech, and Language Processing*, 29:2351–2366, 2021a.
- Liu, C., Wan, Z., Cheng, S., Zhang, M., and Arcucci, R. Etp: Learning transferable ecg representations via ecg-text pre-training. *arXiv preprint arXiv:2309.07145*, 2023a.
- Liu, F., Wu, X., Ge, S., Fan, W., and Zou, Y. Exploring and distilling posterior and prior knowledge for radiology report generation. In *Proceedings of the IEEE/CVF conference on computer vision and pattern recognition*, pp. 13753–13762, 2021b.
- Liu, H., Li, C., Wu, Q., and Lee, Y. J. Visual instruction tuning. *arXiv preprint arXiv:2304.08485*, 2023b.
- Ma, X., Liu, F., Yin, C., Wu, X., Ge, S., Zou, Y., Zhang, P., and Sun, X. Contrastive attention for automatic chest x-ray report generation. *arXiv preprint arXiv:2106.06965*, 2021.
- Moon, S., Madotto, A., Lin, Z., Nagarajan, T., Smith, M., Jain, S., Yeh, C.-F., Murugesan, P., Heidari, P., Liu, Y., et al. Anymal: An efficient and scalable any-modality augmented language model. *arXiv preprint arXiv:2309.16058*, 2023.
- Ouyang, L., Wu, J., Jiang, X., Almeida, D., Wainwright, C., Mishkin, P., Zhang, C., Agarwal, S., Slama, K., Ray, A., et al. Training language models to follow instructions with human feedback. *Advances in Neural Information Processing Systems*, 35:27730–27744, 2022.
- Painter, T. and Spanias, A. Perceptual coding of digital audio. *Proceedings of the IEEE*, 88(4):451–515, 2000.
- Papineni, K., Roukos, S., Ward, T., and Zhu, W.-J. Bleu: a method for automatic evaluation of machine translation. In *Proceedings of the 40th annual meeting of the Association for Computational Linguistics*, pp. 311–318, 2002.
- Qin, H. and Song, Y. Reinforced cross-modal alignment for radiology report generation. In *Findings of the Association for Computational Linguistics: ACL 2022*, pp. 448–458, 2022.
- Radford, A., Wu, J., Child, R., Luan, D., Amodei, D., Sutskever, I., et al. Language models are unsupervised multitask learners. *OpenAI blog*, 1(8):9, 2019.
- Tanida, T., Müller, P., Kaissis, G., and Rueckert, D. Interactive and explainable region-guided radiology report generation. In *Proceedings of the IEEE/CVF Conference on Computer Vision and Pattern Recognition*, pp. 7433–7442, 2023.

- Taori, R., Gulrajani, I., Zhang, T., Dubois, Y., Li, X., Guestrin, C., Liang, P., and Hashimoto, T. B. Alpaca: A strong, replicable instruction-following model. *Stanford Center for Research on Foundation Models*. <https://crfm.stanford.edu/2023/03/13/alpaca.html>, 3(6):7, 2023.
- Touvron, H., Lavril, T., Izacard, G., Martinet, X., Lachaux, M., Lacroix, T., Rozière, B., Goyal, N., Hambro, E., Azhar, F., Rodriguez, A., Joulin, A., Grave, E., and Lample, G. Llama: Open and efficient foundation language models. *CoRR*, abs/2302.13971, 2023a.
- Touvron, H., Martin, L., Stone, K., Albert, P., Almahairi, A., Babaei, Y., Bashlykov, N., Batra, S., Bhargava, P., Bhosale, S., et al. Llama 2: Open foundation and fine-tuned chat models, 2023. URL <https://arxiv.org/abs/2307.09288>, 2023b.
- Vedantam, R., Lawrence Zitnick, C., and Parikh, D. Cider: Consensus-based image description evaluation. In *Proceedings of the IEEE conference on computer vision and pattern recognition*, pp. 4566–4575, 2015.
- Wagner, P., Strodthoff, N., Bousseljot, R.-D., Kreisler, D., Lunze, F. I., Samek, W., and Schaeffter, T. Ptb-xl, a large publicly available electrocardiography dataset. *Scientific data*, 7(1):154, 2020.
- Wan, Z., Yin, Y., Zhang, W., Shi, J., Shang, L., Chen, G., Jiang, X., and Liu, Q. G-map: general memory-augmented pre-trained language model for domain tasks. *arXiv preprint arXiv:2212.03613*, 2022.
- Wan, Z., Liu, C., Zhang, M., Fu, J., Wang, B., Cheng, S., Ma, L., Quilodrán-Casas, C., and Arcucci, R. Med-unic: Unifying cross-lingual medical vision-language pre-training by diminishing bias. *arXiv preprint arXiv:2305.19894*, 2023a.
- Wan, Z., Wang, X., et al. Efficient large language models: A survey. *arXiv preprint arXiv:2312.03863*, 2023b.
- Wang, B. and Komatsuzaki, A. GPT-J-6B: A 6 Billion Parameter Autoregressive Language Model. <https://github.com/kingoflolz/mesh-transformer-jax>, May 2021.
- Wang, J., Li, R., Li, R., Li, K., Zeng, H., Xie, G., and Liu, L. Adversarial de-noising of electrocardiogram. *Neurocomputing*, 349:212–224, 2019.
- Wang, X., Wan, Z., Hekmati, A., Zong, M., Alam, S., Zhang, M., and Krishnamachari, B. Iot in the era of generative ai: Vision and challenges. *arXiv preprint arXiv:2401.01923*, 2024.
- Wang, Y., Ivison, H., Dasigi, P., Hessel, J., Khot, T., Chandu, K. R., Wadden, D., MacMillan, K., Smith, N. A., Beltagy, I., et al. How far can camels go? exploring the state of instruction tuning on open resources. *arXiv preprint arXiv:2306.04751*, 2023.
- Wei, J., Tay, Y., Bommasani, R., Raffel, C., Zoph, B., Borgeaud, S., Yogatama, D., Bosma, M., Zhou, D., Metzler, D., et al. Emergent abilities of large language models. *arXiv preprint arXiv:2206.07682*, 2022.
- Wolf, T., Debut, L., Sanh, V., Chaumond, J., Delangue, C., Moi, A., Cistac, P., Rault, T., Louf, R., Funtowicz, M., et al. Huggingface’s transformers: State-of-the-art natural language processing. *arXiv preprint arXiv:1910.03771*, 2019.
- Wolf, T., Debut, L., Sanh, V., Chaumond, J., Delangue, C., Moi, A., Cistac, P., Rault, T., Louf, R., Funtowicz, M., Davison, J., Shleifer, S., von Platen, P., Ma, C., Jernite, Y., Plu, J., Xu, C., Scao, T. L., Gugger, S., Drame, M., Lhoest, Q., and Rush, A. M. Transformers: State-of-the-art natural language processing. In *Proceedings of the 2020 Conference on Empirical Methods in Natural Language Processing: System Demonstrations*, pp. 38–45, Online, October 2020. Association for Computational Linguistics. URL <https://www.aclweb.org/anthology/2020.emnlp-demos.6>.
- Workshop, B., Scao, T. L., Fan, A., Akiki, C., Pavlick, E., Ilić, S., Hesslow, D., Castagné, R., Luccioni, A. S., Yvon, F., et al. Bloom: A 176b-parameter open-access multilingual language model. *arXiv preprint arXiv:2211.05100*, 2022.
- Wu, Y., Rabe, M. N., Hutchins, D., and Szegedy, C. Memorizing transformers. *arXiv preprint arXiv:2203.08913*, 2022.
- Zhang, S., Roller, S., Goyal, N., Artetxe, M., Chen, M., Chen, S., Dewan, C., Diab, M., Li, X., Lin, X. V., et al. Opt: Open pre-trained transformer language models. *arXiv preprint arXiv:2205.01068*, 2022.
- Zhang, S., Dong, L., Li, X., Zhang, S., Sun, X., Wang, S., Li, J., Hu, R., Zhang, T., Wu, F., et al. Instruction tuning for large language models: A survey. *arXiv preprint arXiv:2308.10792*, 2023a.
- Zhang, T., Kishore, V., Wu, F., Weinberger, K. Q., and Artzi, Y. Bertscore: Evaluating text generation with bert. *arXiv preprint arXiv:1904.09675*, 2019.
- Zhang, X., Zhang, D., Li, S., Zhou, Y., and Qiu, X. Speech-tokenizer: Unified speech tokenizer for speech large language models. *arXiv preprint arXiv:2308.16692*, 2023b.
- Zheng, R., Chen, J., Ma, M., and Huang, L. Fused acoustic and text encoding for multimodal bilingual pretraining and speech translation. In *International Conference on Machine Learning*, pp. 12736–12746. PMLR, 2021.

Zhu, D., Chen, J., Shen, X., Li, X., and Elhoseiny, M.
Minigt-4: Enhancing vision-language understanding
with advanced large language models. *arXiv preprint
arXiv:2304.10592*, 2023.

A. Hyper-parameters of ECG Instruction Tuning

Table 4. Hyper-parameters of ECG instruction tuning for all LLM backbones.

| Hyperparameters | |
|---------------------------|------------|
| Mixed precision | bf16 |
| Instruction tuning epochs | 5 |
| LoRA alpha | 64 |
| LoRA rank | 128 |
| LoRA dropout | 0.1 |
| Total batch size | 64 |
| Gradient accumulation | 2 |
| Maximum sequence length | 256 |
| Learning rate | 2e-5, 1e-4 |
| Learning rate Optimizer | AdamW |
| Schedule | linear |
| Warm-up ratio | 0.03 |
| Weight decay | 0.0 |

Table 5. ECG dimension of different language models.

| MODELS | ECG Dimension |
|------------------|---------------|
| GPT2-Medium | 64 |
| GPT2-Large | 64 |
| GPT-Neo | 128 |
| GPT-NeoX | 96 |
| GPT-J | 256 |
| BLOOM | 128 |
| OPT | 128 |
| LLaMA-1 | 128 |
| Mistral | 128 |
| LLaMA-2 | 128 |
| Mistral-Instruct | 128 |

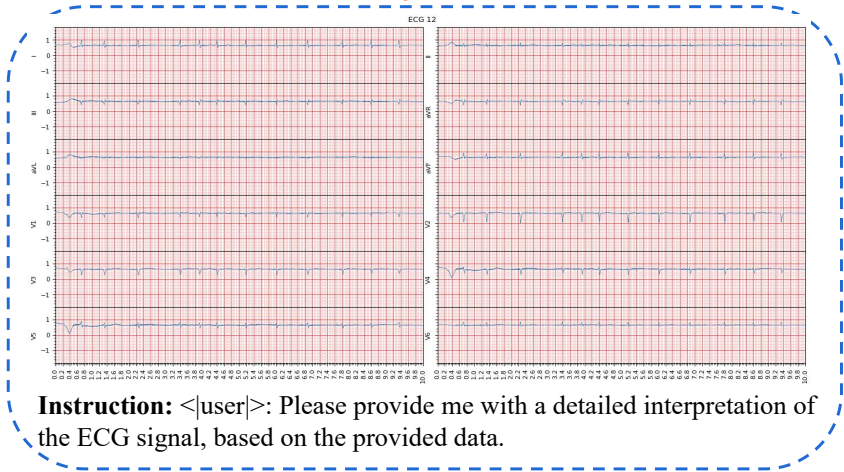
In this study, we concentrate on the implementation of the Low-Rank Adaptation (LoRA) (Hu et al., 2021) technique for efficient fine-tuning, specifically applied to ECG instruction tuning. As detailed in Table 4 provided, we utilize mixed precision at bf16 for enhanced computational efficiency. Our models undergo instruction tuning over 5 epochs, with LoRA parameters set at an alpha of 64 and a rank of 128, accompanied by a dropout rate of 0.1. The total batch size is 64 with a gradient accumulation factor of 2. The maximum sequence length is constrained to 256 tokens. Additionally, we adopt a learning rate with 2e-5 for GPT-NeoX, and 1e-4 for the other models, optimized using the AdamW algorithm. The learning rate follows a linear schedule with a warm-up ratio of 0.03. We set the weight decay to 0.0.

Moreover, as shown in Table 5, we detail the ECG embedding dimensions for various language models, highlighting their approach to ECG data encoding. GPT2-Medium and GPT2-Large feature ECG dimensions of 64, while GPT-Neo, BLOOM, OPT, LLaMA-1, Mistral, LLaMA-2, and Mistral-Instruct use a dimension of 128. GPT-NeoX employs a dimension of 96, and GPT-J notably uses the largest dimension of 256. These dimensions, reflecting each model’s head dimension design, illustrate diverse strategies in ECG data processing across different models.

B. Visualization of Generated ECG Report Samples

As illustrated in Figures 9, 10, and 11 we have visualized the report samples generated by LLaMA-1, LLaMA-2, and Mistral-Instruct. The samples are presented in blue font to highlight the key information that aligns with the ground truth. The visualization demonstrates that all three selected models are capable of capturing the essential patterns of ECG signals and generating accurate reports. This underscores the efficacy of our proposed MEIT framework, which proves to be adaptable to the majority of open-source LLMs. It effectively learns the correct clinical semantics of ECG signals, thereby enabling the generation of corresponding reports.

LLaMA-1



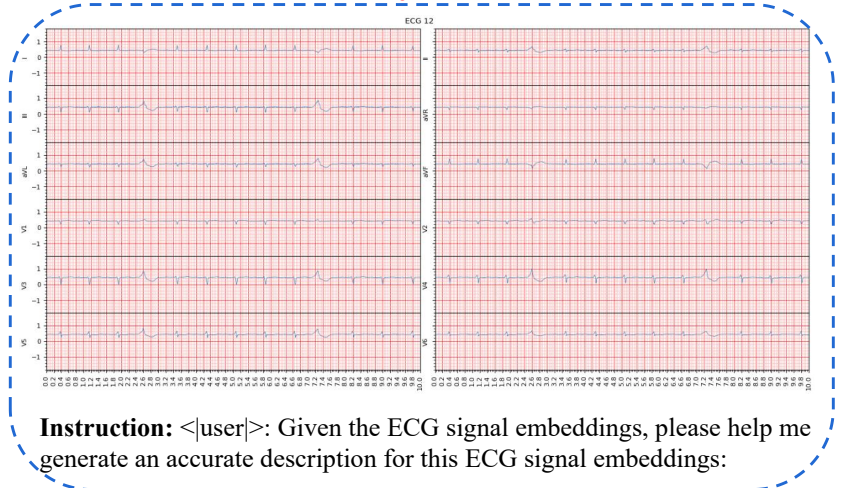
Instruction: <|user|>: Please provide me with a detailed interpretation of the ECG signal, based on the provided data.

Generated Report: <|assistant|>: atrial fibrillation. extensive st-t changes may be due to myocardial ischemia. abnormal ecg.</s>

Ground Truth: <|assistant|>: atrial fibrillation. possible inferior infarct - age undetermined. possible anteroseptal infarct - age undetermined. lateral st-t changes may be due to myocardial ischemia. abnormal ecg.</s>

Figure 9. Reports generated by LLaMA-1 following ECG instruction Tuning.

LLaMA-2



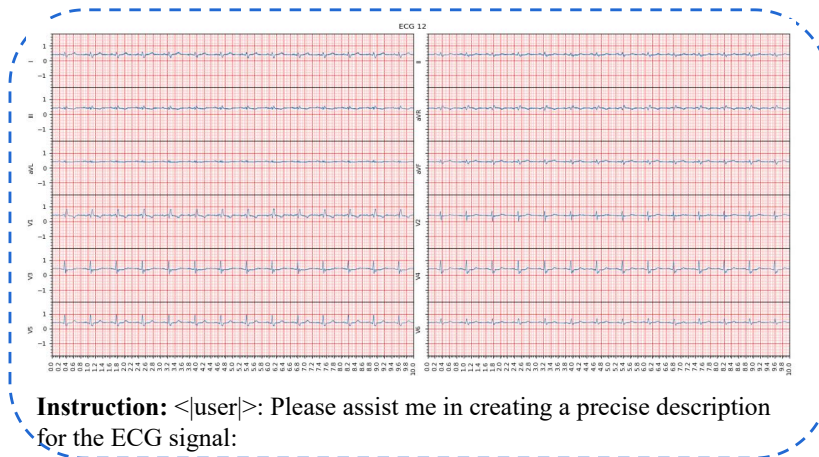
Instruction: <|user|>: Given the ECG signal embeddings, please help me generate an accurate description for this ECG signal embeddings:

Generated Report: <|assistant|>: sinus rhythm with 1st degree a-v block. left axis deviation. left ventricular hypertrophy. inferior/lateral st-t changes may be due to hypertrophy and/or ischemia. abnormal ecg. </s>

Ground Truth: <|assistant|>: sinus rhythm with 1st degree a-v block. left axis deviation. probable normal variant. inferior/lateral st-t changes may be due to myocardial ischemia. abnormal ecg. </s>

Figure 10. Reports generated by LLaMA-2 following ECG instruction Tuning.

Mistral-Instruct



Instruction: <|user|>: Please assist me in creating a precise description for the ECG signal:

Generated Report: <|assistant|>: sinus rhythm. right bundle branch block. abnormal ecg.</s>

Ground Truth: <|assistant|>: sinus rhythm. indeterminate axis. right bundle branch block. abnormal ecg. </s>

Figure 11. Reports generated by Mistral-Instruct following ECG instruction Tuning.